Available online at www.sciencedirect.com
ScienceDirect
Cement and Concrete Research 37 (2007) 1321 – 1333
Cement and Concrete Research

Mixing of concrete or mortars: Dispersive aspects

Pierre-Henri Jézéquel *, Véronique Collin

Lafarge Centre de Recherche, (Groupe Interactions Matériau-Procédé) 95, rue du Montmurier, B.P.15, 38291 Saint Quentin Fallavier Cedex, France

Received 2 October 2006; accepted 21 May 2007

Abstract

This article describes an experimental methodology offering mixing efficiency criteria for granular materials in terms of their dispersion capability. This methodology is based on the analysis of the dispersion kinetics of colored, cohesive, tracer particles that progressively disagglomerate during stirring. The effects of certain critical parameters such as the mixer speed and the type of mixer are described. In terms of the mix design, the contribution of the largest particles to the dispersion kinetics, and therefore to the mixing efficiency, is highlighted. A simple comparison of the mixing efficiency of mixer/mix design/procedure sets is finally provided for such cementitious granular materials.

Keywords: Dispersion; Fresh concrete; Mixing

1. Introduction

The impact of mixing for such construction materials as mortar and concrete can be very significant and affect their final properties. Due to their granular structure, concrete or mortars are special materials, made up of an assembly of particles of different sizes ranging from typically less than a few microns up to a few centimeters. In these materials, rheology and porosity are controlled through the granular composition of a wide variety of cements, sands, fillers and aggregates of different chemical compositions, mean sizes, size dispersions, shapes, densities, surface properties, etc. Mixing these particles together with water to produce a homogeneous mixture could become an industrial challenge when considering the fact that productivity is directly related to the mixing time. This is in the 30–60 s range for a standard concrete and can reach 10 min for a high performance concrete.

The efficiency of the mixing operation is often determined by the homogeneity of the produced concrete. For instance, technical associations such as RILEM [1], or even standards, define the efficiency of a mixer as its capability to "uniformly distribute all its constituents in the container without favoring one or the other". This homogeneity is measured from batch to batch either by evaluation of the variability of the concrete composition, a very tedious task, or by the variations of product homogeneity based on dependent macroscopic properties (strength, rheological characteristics, etc.). Several authors [2–4] have described such approaches, but all have expressed reserves concerning the validity of the sampling, that was extensively studied by Robin [5]. The industrial approach of mixing efficiency merely deals with energy considerations. Batch concrete mixers are equipped with wattmeters that are supposed to measure, but in fact only estimate, the temporal evolution of the electrical power supplied to the mixers motors to maintain speed. Power increases dramatically during the very first moments after the water addition, at the same time as the interparticulate forces become predominant during the water percolation inside the porous network formed by the granular assembly. These forces are mainly capillary forces, but cement also reacts immediately upon contact with water and starts forming hydrates [6]. At this time, the mixture looks like a wet granular material. When all the water is integrated in the network the relative motion of the particles is favored, and the shear forces overcome the interparticulate forces; the particle agglomerates are progressively broken and the entrapped water is freed, enabling the smaller particles to fill the intergranular voids. The power drops until the smallest aggregates are broken, so that the power finally reaches a steady state. It is often considered that mixing is then over. The stabilization time required for a given mixer to reach mixing

* Corresponding author. Tel.: +33 474828177; fax: +33 474821850.
E-mail address: pierre-henri.jezequel@lafarge.com (P.-H. Jézéquel).

0008-8846/$ - see front matter © 2007 Elsevier Ltd. All rights reserved.
doi:10.1016/j.cemconres.2007.05.007

completion was related to the composition of the concrete and more specifically, but not exclusively, to the maximum packing fraction as well as to the real packing fraction [5]. However, it could not be directly linked to the homogeneity of the final concrete.

When considering concrete or mortar mixing, it is useful to separate the largest particles, i.e. the aggregates, and the rest of the ingredients, i.e. the smallest particles and water. The aggregates are distributed in the mixing vessel faster that the other components [2]. They also play a very active role in mixing efficiency and, although this has been observed by the experts in the field such as Powers [8] who mentions that "the rolling mass of aggregates in the concrete mixer homogenizes the paste as effectively as the most vigorous laboratory stirrer", this is not clearly documented in the literature. The relative motion of the aggregates creates local and transient "micro-mixers" acting on the evolving slurry formed by the smallest particles and the water located between the aggregates. These "micro-mixers" not only favor the distribution of the smallest particles, but are also responsible for the rupture of the links between the small particles. The local and transient shear or frictional forces are the mechanisms involved in this dispersive action. These are depending on the characteristics of the particles and on the mean distance between the aggregates, as well as on the collisions, characterized by their frequency and their kinetics energy, which are affected by the geometry and the speed of the mixer.

Mixing achieves both distributive and dispersive tasks which operate simultaneously or consecutively. In certain mix designs, particularly standard concretes, it is generally accepted that the particles are not significantly agglomerated after mixing, suggesting that the dispersion process is efficient. This is probably why no study presents dispersion-related results in the literature on concrete, whereas this is more frequent in other industries [9]. For more sophisticated mix designs that contain very small particles, dispersion becomes a limiting task because of the interparticulate forces which depend on the inverse of the particle size. A priori, there is no argument why a mixer would perform similarly in both tasks, so that the question of mixing efficiency must consider almost independently the efficiency of the two mechanisms.

The objective of the study is the development of robust indicators for mixing efficiency of granular materials aiming at better understanding of concrete mixing. Despite it was studied simultaneously, it is not the purpose of the present paper to describe the distribution capability of (mixer/mix design) sets. The paper describes methodological aspects pertaining exclusively to characterization of the dispersion efficiency. However, it does not characterize the homogeneity of the mixture nor the true material's level of dispersion; this would have required to extract and analyze reproducibly the intergranulate slurry, which is difficult, tedious and poorly reproducible. Therefore this is only the capability of the (mixer/mix design) pair to achieve dispersion of small elements that was characterized. Considered another way, the capability to describe dispersion could also open opportunities to better evaluate the solicitations that are imposed to the granular material at a micro-scale whose characteristic size is the mean distance between aggregates. The use of cohesive colored tracer particles, progressively disagglomerated under shear or frictional forces, was selected as the technique of choice. Because the proposed technique does not measure the true level of dispersion of the small particles of the mix, it must be made very clear that it only allows to make relative comparisons of the influence of the granular mix design or of the mixing process on the dispersion capability, but cannot provide absolute pieces of information unless a careful calibration is achieved.

2. Methodology development

2.1. Choice of the tracers

In order to characterize only the dispersion capability of mixer/mix design pairs, it is necessary not to be strongly affected by the distributive aspects concurrently taking place. As mentioned earlier, the straightforward measurements of one or both mechanisms is either very tedious, even impossible with the usually available industrial tools, since these mechanisms are particle dependent. Therefore, alternatives to analyze the product during mixing had to be found. Our choice was to investigate the interest of using specific particles with at least two characteristics:

- their capability to be distributed and/or dispersed could be easily varied,
- the state of particle dispersion or distribution could be relatively easily detected, even in industrial situations.

Despite the many potential systems meeting these requirements, very few were explored for this purpose. After careful screening of alternative solutions, we decided to use tracer particles, in the form of colored aggregated objects added to the mix design at low concentration levels. The main reason for this choice was that any other detectable characteristics than color was either much more difficult to measure accurately or they led to intense efforts to generate the particles (for example, radioactive tracers are used by Vandanjon et al. [3]).

The selected colored aggregated objects were red iron oxide pigments. Bayer® manufactures a series of particles containing the same reference particles (iron oxide particles Bayferrox 110 synthesized by Lanxess®), but their level of aggregation varies because of a different manufacturing process. The series can be summarized as follows:

- 110 P: powder made of *individual* Bayferrox 110 particles (size 90 nm, density 5.0).
- 110 C: powder made of *compacted* Bayferrox 110 particles (size 40 μm).
- 110 G: powder made of *granulated* Bayferrox 110 particles (size 100 μm, density 1.4).

110P is a usual pigment powder containing non-agglomerated sub-micron particles. These can be used as tracers, for instance to evaluate the distribution capability of small and dense particles. They are useless however to evaluate dispersion. 110C and 110G are both made of cohesive particles. More

specifically, they appear as spherical aggregates with diameters varying between a few microns for the former and approximately 400 μm for the latter. Fig. 1 shows an example of both the 110C and 110G granules and the corresponding individual particles.

Because of their use in concretes and mortars, that are possibly highly admixtured products, we validated that these materials do not greatly interfere with water reducers or rheology enhancers for instance, and that they can be used at low concentrations without greatly modifying the granular compositions. In this respect, any of the three types of 110 particles behaved much better than most of the other commercial pigments in different colors (yellow or green pigments for instance, [7]), probably because their spherical shape lowered their surface area. Amounts as small as 0.4 to 0.8% (mass ratio/total solids) in a granular mixture can be easily detected with a colorimeter.

The selection between compacted 110C and granulated 110G for the tracers could have been based only on their disagglomeration kinetics, developed later in this paper. Disagglomeration of 110C during mixing is much faster than 110G because of the lower interaction forces between the individual pigment particles, and there was significant competition with the kinetics of the individual particle distribution throughout the mixer. In addition, the compaction process was less well controlled, and we observed important batch to batch variability for 110C. This was much more reduced for 110G. Therefore, 110G is the choice tracer.

It might be argued that the use of iron oxide pigments to quantify the dispersion phenomena in mixers cannot be fully justified by kinetic considerations, since the mode and kinetics of dispersive mixing processes are related to the strength of the shear field or of the frictional effects relative to the cohesion of the solids being dispersed. In this case, quantitative information on the cohesiveness of the pigments or the material within the concrete mix that is subject to dispersive mixing would be required. However, it is well known that material property consistency including mechanical strength of agglomerates can be quite poor, so that a rigorous characterization of the absolute cohesiveness was unlikely to be successful. If the tracer pigments are less cohesive than the concrete solids, the interpretation of pigment dispersion observed in the experiments might not be relevant to dispersion of the concrete solids. This is probably not the case with the pigment 110G, because of the relatively high characteristic times required for its dispersion. If the pigments are more cohesive than the concrete solids, then dispersion of the sensitive concrete ingredients can occur before it would be noticeable with the pigments. Our intent is to remain purposely under such conditions, and we do not consider that this is detrimental because:

- the competition between distribution and dispersion requires that the tracer behaves very differently with this respect in order to be able to separate clearly the two effects. Dispersion of 110G is much slower than distribution. Therefore, we do not use the dispersion times of the pigments as direct measures of the dispersion times of cement,
- means of quantifying the effect of powder clusters cohesiveness on color kinetics responses can be defined, even though the true cohesiveness of these pigment clusters is not measured.

There are significant differences between the physical characteristics of cement and iron oxide pigment particles (for example, density, shape, cohesiveness…). Considering density only, we can point out that the agglomerate 110G is much less dense (density = 1.4) that the density of the disagglomerated individual particles (typically density = 5.0). It is also the case for concrete, for which the density of the agglomerated and the individual particles differ. Despite these differences, the pigments can be considered anyway as active tracers of the local solicitations that are imposed by the (process/mix design) pair to the cement particles that are necessarily concretes or mortars constituents, but this does not mean that their dispersion capability is the same. Finally, despite the fact that shear, shocks and friction are, at different levels, responsible for de-agglomeration of particles, no certitude exists that the de-agglomeration mechanisms for the pigment are the same as for the cement in all the experimental situations. Unfortunately, the possibility to bring clear experimental elements to justify the equivalence is beyond the scope of the present paper.

It must also be mentioned that the methodology is not relevant, without change, for the analysis of the important mixing stage which is the dry–wet transition corresponding to the paste formation. Since the tracer is introduced once the paste is formed, the presented techniques potentially qualify only the ability of the

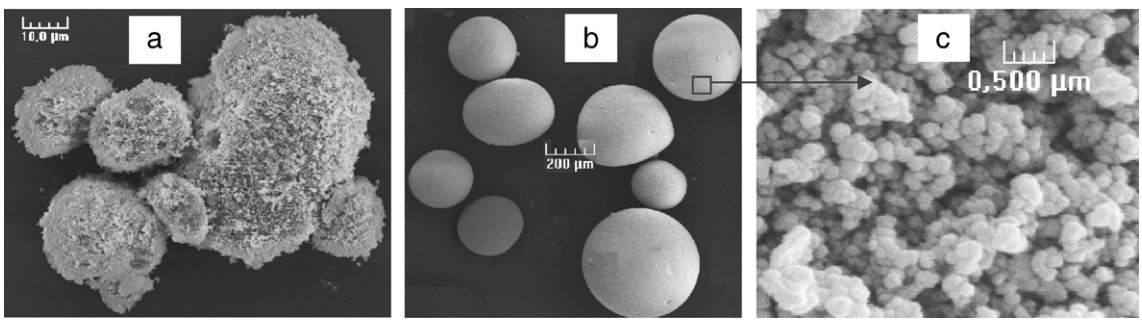

Fig. 1. (a) SEM picture of 110C aggregates. (b) SEM picture of 110G aggregates. (c) SEM picture of elementary pigment particles in 110C or 110G aggregates.

mixers to introduce shear in a fluid-like material. The performance of the mixers before the dry to wet phase transition could possibly be different of what it is after the material becomes fluid.

2.2. Experimental protocol

Although concretes and mortars can be industrially prepared several ways that take productivity considerations into account, the preparation protocol is much more precisely defined at the laboratory scale:

(1) Introduce sands (and gravels for concrete) in the mixer.
(2) Introduce part R_1 of the water for pre-wetting, and stir for 30 s at Ω_1 rpm.
(3) Wait 4 min, until the largest particles have absorbed water.
(4) Add hydraulic binders (cements or mineral additives), and stir for 1 min at Ω_1 rpm, so that all the particles are homogenized before water addition.
(5) Add the rest R_2 of the water in 30 s while stirring at Ω_1 rpm,
(6) Stop stirring, and add pigment powder,
(7) Resume stirring at Ω_2 rpm for a variable time depending on the color evolution.

Ω_1 and Ω_2 are mixer and volume dependant, but Ω_1 is generally lower than Ω_2. R_1 and R_2 are material dependant.

Time $t=0$ begins at step 5. The optimal time for the pigment powder addition is during step 6 rather than being premixed with the cement powder, because pre-mixing the dry powders initiates pigment disagglomeration before any wet mixing takes place. The pigment is introduced in 30 s. It is homogeneously spread on the top of the free surface. Let us mention the fact that sensitivity of the methodology increases as the optical contrast between the medium and red particles increases. Although this is not a prerequisite, white cement could replace customary grey cement. In the protocol described above, mixing is often prolonged much longer than what is customary suggested for mixing similar products.

As time progresses, the particles are rapidly distributed (characteristic time is lower than 30 s), and the average color of the mix evolves because the particles de-aggregate under the influence of mixing. The number of particles is no longer constant over time. The largest particles are progressively destroyed and small particles continuously appear. This contributes to increasing the light diffusion until all the aggregated particles initially added to the granular mix design are destroyed.

The average red color depends mainly on the number of diffusive centers, and is a function of the concentration of individual disagglomerated pigment particles per volume unit. The evolution of the average color can be quite easily monitored with a pre-calibrated colorimeter (Dr. Lange Micro Color II). The best way of characterizing the color is to follow the recommendations provided by the CIE [10] and use the tridimensional color model CIE1976L*a*b*. Its advantage is of representing the perceptions of the color differences in a uniform and linearized way. Because of the clear red color of the iron oxide pigments, parameter a* (the red/green axis of the L*a*b* space) alone can characterize the color of the mixture. A few cm^3 of the mixture can be withdrawn from mixer. The largest gravel particles, if any, are removed so that the 2-cm cells of the colorimeter are accurately filled with a mortar–equivalent mixture in a reproducible manner. Reading of a* is immediate. Assuming a relatively homogeneous medium, no more than 3 samples could be taken, one in the center, one at half radius and one close to the wall of the mixing vessel. The values are then averaged. The accuracy of the determination of the individual a* values is typically lower than 1% for a given colorimeter, even though it is difficult to obtain reproducible results with different colorimeters.

The evolution of the mean color in series of samples is measured at regular time intervals. Fig. 2 shows the experimental evolution of parameter a* over time (the so-called "color kinetics") for a standard laboratory "planetary" mixer (MM1) operating at 280 rpm. The product mixed in this example is 1 l of "plastic" mortar containing 0.8% of 110G. The term "plastic" describes the consistency of the material, by opposition to "fluid" or "firm". These words can be linked to rheological characteristics defined, for instance, by Struble [11].

One can easily observe that the raw results are well fitted by the exponential kinetic law given below:

$$a^*_t = a^*_{max} + (a^*_{min} - a^*_{max}) \times \exp(-t/t_c), \quad (1)$$

a^*_{max} is the maximum value of a* vs. time curve. It only depends on the amount of coloring particles added. a^*_{min} corresponds to the virtual minimum value of a* obtained if the coloring particles are perfectly distributed at time $t=0$. The span (a^*_{max}–a^*_{min}) is an indicator of the sensitivity of the experimental method. It must be maximized.

t_c is a characteristic dispersion time for 110G. This is the choice criteria for comparing the performances of the mix design/mixer pairs. Series of reproducibility experiments have

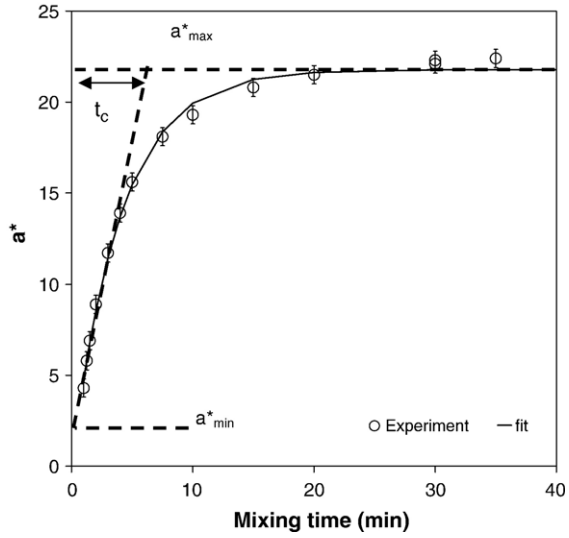

Fig. 2. Evolution of a* over time during stirring. MM1 mixer, 1l, 280 rpm, 0.8% 110G particle, "plastic" mortar containing particles no larger than 4 mm. Mix design: mixture #2, described in Appendix A.

demonstrated that t_c is known for the same process/mix design with a precision lower than 5%.

2.3. Modes of evolution of the tracer particles

In order to be able to link color and solicitations applied to the particles, it is now necessary to better understand how the most pigment clusters disagglomerate during mixing. The fracture of the iron oxide clusters could result from one or several of the disagglomeration modes (Fig. 3) already described by Rwei et al. [12] and Collin and Peuvrel-Disdier [13]:

– *erosion,* which regularly produces small particles,
– *rupture*, which suddenly produces relatively large particles,
– *crushing*, which brutally produces small particles,

Because it is impossible to observe the behavior of pigment clusters directly inside mortars or concretes, the 110G particles were first examined in a transparent model medium to overcome this problem. Several viscous solutions of glucose (up to 50 Pa s) were prepared and placed in the gap of a transparent plate–plate rheometer, to impose steady shear rates (as high as 50 s^{-1}). It was not possible to observe any degradation of the 110G granules because the stress imposed by the shear of glucose alone was lower than the high yield cohesion stress of the pigment clusters. When transparent glass beads (SOVITEC AF, radius 75 μm) were added at high concentrations to the glucose solutions, erosion and crushing was observed, but no rupture. Erosion was mainly generated by friction with the other solid constituents. While many causes can provoke rupture (intense shear or elongational stresses or even shocks), it is believed that shocks between particles are mainly responsible for crushing. If it is assumed that glass beads behave like sand grains and that glucose is equivalent to the cement paste, one can presume that the pigments dispersion mode in mortars and concrete will also be a combination of erosion and crushing.

Several erosion laws are advanced in the literature [14–16], but the most frequently used laws consider that the rate of reduction of the cluster size R_t is proportional to the local shear stress $\sigma = \eta\dot{\gamma}$ applied and to the size of the cluster. Assuming that erosion is the only mechanism involved, we obtain (in the Eqs. (2)–(6), the sign $\propto$ indicates the proportionality between the two terms):

$$\frac{dR_t}{dt} \propto -\eta\,\dot{\gamma} \times R_t, \tag{2}$$

which gives after integration:

$$\frac{R_t}{R_0} \propto \exp[-k\sigma \times t], \text{ with } \sigma = \eta\,\dot{\gamma}, \text{ and } k\ a \text{ constant} \tag{3}$$

Despite the fact that a^* is an indicator of the presence of the fine particles that diffuse light, it is still logical to assume that, at time t, $a^*_{max} - a^*_t$ is proportional to the amount available for erosion between time t and t_∞ and is thus proportional to R_t. Similarly, $a^*_{max} - a^*_{min}$ is proportional to the total amount to erode, and is proportional to the initial cluster size. Eq. (2) can thus be rewritten as:

$$\frac{a^*_{max} - a^*_t}{a^*_{max} - a^*_{min}} \propto \exp[-k\sigma \times t] \tag{4}$$

Similar arguments could be invoked for crushing, providing the particle size is replaced by the number of clusters per volume unit Nb^r_t remaining to be crushed at time t. The evolution of Nb^r_t is proportional to the evolution of the number of debris Nb^c_t resulting from previous crushing, and from a parameter λ whose magnitude depends on the solicitation leading to crushing.

$$\frac{dNb^r_t}{dt} \propto -\frac{dNb^c_t}{dt} \propto -\lambda \times Nb^r_t \tag{5}$$

We can assume that $a^*_{max} - a^*_t$ is also proportional to the number of particles to be crushed between time t and $t\infty$ and that $a^*_{max} - a^*_{min}$ is proportional to the total number of particles. Thus, Eq. (5) leads to exponential behavior for crushing as well:

$$\frac{a^*_{max} - a^*_t}{a^*_{max} - a^*_{min}} \propto \exp[-k_2\lambda \times t] \tag{6}$$

where k_2 is a proportionality constant.

Eqs. (4) and (6) suggest that the exponential behavior of a^* over time is not discriminating to one of these mechanisms. Erosion and crushing are compatible with such experimental results as those obtained in Fig. 2 and Eq. (1).

In order to make progress and determine which mechanism is predominant, another experimental approach was necessary. Color kinetics experiments with 110G were first done on a mortar mix design using a 1-l laboratory MM1 mixer. Samples were regularly withdrawn and allowed to harden in cylinders. Each of these samples was precisely cut in 10 slices and the surfaces polished and analyzed with an optical microscope to evaluate the density of the uncrushed particles (the elementary particles could not be observed and were not taken into account). The percentage of surface area S2 occupied by the uncrushed particles was thus measured by image analysis. The

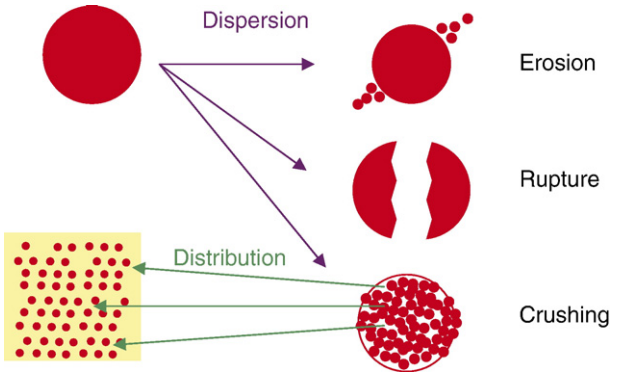

Fig. 3. Fragmentation and distribution modes for cohesive tracer particles.

variation of the number of uncrushed particles over time was expressed for these samples by:

$$\frac{dNb_t^r}{dt} = \frac{dNb_t^r}{da_t^*} / \frac{da_t^*}{dt} \quad (7)$$

The two terms on the right side of Eq. (7) could be evaluated separately. The color kinetics in Fig. 2 directly provides the time derivative of a^* for each time period, but the numerator of Eq. (7) requires calibration. For this purpose, 400 110G particles were placed in seven cups. In each cup, a known, but variable, number of clusters were hand crushed. Exactly the same amount of identical cement paste was subsequently added to each cup and gently hand mixed to ensure distribution of the coloring particles. a^* was measured for each mix to access a^* versus Nb_t^r. There is a linear relationship, because $\frac{dNb_t^r}{da_t^*}$ is constant (Fig. 4). $\frac{dNb_t^r}{dt}$ and eventually Nb_t^r could then be determined from Eq. (7) and compared with the values of the bi-dimensional surface area S2 obtained from direct observations of the samples generated in the mortar mixer. Fig. 5 summarizes this comparison.

These results show that the number of grains left Nb_t^r is linearly linked to the total surface S2 of the red particles. For each sample, $S2 = 4\Pi R_t^2 Nb_t^r$/total sample surface. The linear relationship is only possible if the radius of the clusters R_t remains almost unchanged, assumption that is problematic to confirm experimentally by direct evaluation of the particle size by image analysis. Based on the invariance of R_t, we can conclude that the dominant mechanism for dispersion of 110G is crushing. If we cannot exclude that some erosion could occasionally relay crushing, with a slower and much less efficient kinetics, it is highly unlikely that erosion could become significant for media either containing large particles or being very concentrated.

2.4. Influence of cluster cohesion on color kinetics

Since it is necessary to have a tracer much more sensitive to dispersion than to distribution, it was important to determine how the color kinetics curves deal preferentially with dispersion rather than with distribution. Experiments at several mixer rotation speeds can differentiate between the two effects. The dependency of a^* vs. mixing time curves on the mixer speed Ω (Fig. 6a) explains the sensitivity to the process, but cannot provide directly usable information on the mechanisms involved, because the deformation $n_t = \Omega.t$ applied to the mixture is the main driver of distribution. If the pigments were only distributed inside the medium and not dispersed, we would find independence between the a^* vs. deformation curves and the mixer speed Ω. This independence is found for non cohesive particle, such as 110P. It was not observed in Fig. 6b, that plots the effects of the mixer speed for 110G versus the two parameters N and n_t; the higher the speed the higher the color kinetics for a same number of rotations done by the mixer. When Ω increases, the mean stress applied to the cohesive particles increases as well as the probability of exceeding the yield of cohesion. The dispersion mechanism becomes more efficient.

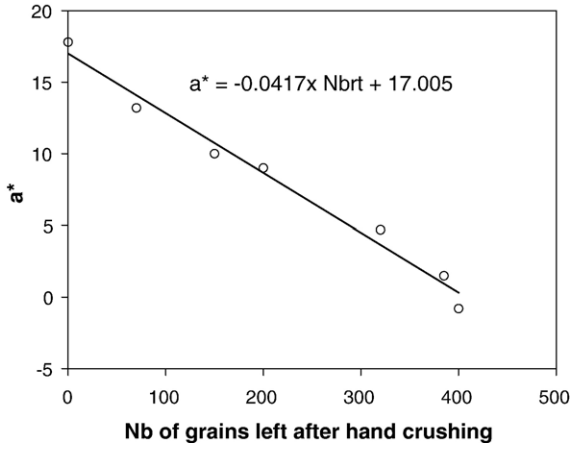

Fig. 4. Calibration of the relationship between color a* and the number of non-crushed particles Nb_t^r.

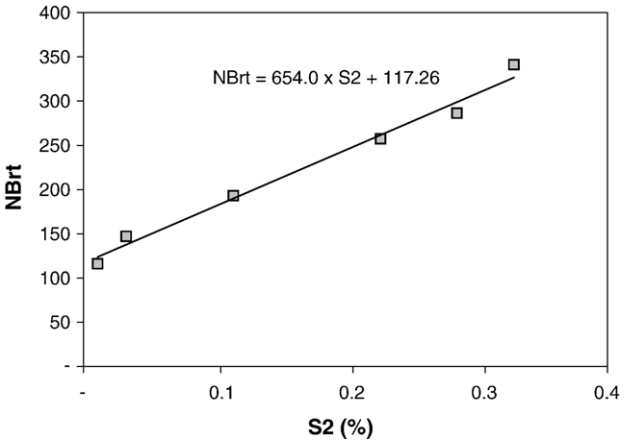

Fig. 5. Relationship between the number of non-crushed particles Nb_t^r and the surface S2 of the particles, obtained after observations with an optical microscope.

When comparing the two curves for the two other powders of the 110 series, whose cohesion was degraded or inexistent, the results were different, as expected (Table 1). By doubling the mixer speed with 110P, there was a reduction of the characteristic time by a factor of about 2, whereas t_c dropped respectively by a factor of about 3.6 and 5.0 for 110C and 110G. In addition, the gap between the a^* vs. deformation curves at the same mixer speeds (140 and 280 rpm) decreased from 110G to 110C to 110P. This confirmed the fact that dispersion was not the dominant mechanism with the non-cohesive powder, whereas the evolution of a^* for 110C was due to both dispersion and distribution. In addition to validate the choice of the 110G tracer, these observations show that it would be possible to find a means of quantifying the effect of powder clusters cohesiveness on color kinetics responses.

Based on the information gathered at two mixer speeds, we could thus define a cohesion index i_c for the powders. Defining $r_{ij} = \frac{t_c^{N_i}}{t_c^{N_j}}$ as the ratio of the characteristic times at two different mixer speeds and $v_{ij} = \frac{\Omega_j}{\Omega_i}$ as the ratio of these mixer speeds, the cohesion index i_c is expressed as:

$$i_c[\text{cluster}] = \frac{r_{ij}}{v_{ij}} = \frac{t_c^{N_i}/t_c^{N_j}}{\Omega_j/\Omega_i} \quad (8)$$

when i_c is close to 1, the main mechanism is distribution and t_c is close to zero, whereas higher values indicate that the dispersive mechanisms become more and more predominant as cohesion progresses. i_c is mainly depending on the nature of the cohesive particles and, even though it is defined for a particular mixing process, it is not highly depending on this process.

3. Experimental results

This chapter first describes certain effects of important mix design parameters such as the particle size and the volume fraction of solids. The role of the process will be presented through the dominant effect of the mixer's speed, and some examples of the impact of the mixer's geometry will be eventually considered.

3.1. Effect of the nature of the granular material

Series of experiments were carried out in order to compare the mixing efficiency of standard mortars and concretes in the same mixer, frequently used for concrete mixing (CM2 mixer, volume = 30 l, mixer speed = 55 rpm). Professional civil engineers know how to formulate mortars at the laboratory scale and concretes at a higher scale so that their critical rheological and mechanical properties are the same, but the description of the approaches used is an issue out of the scope of this paper. The materials selected for the rest of this study were closely connected, since the selected mortar was a reference laboratory scale formula used for industrial concrete (typical mix designs used are described in Appendix I). The color kinetics curves of the two materials (Fig. 7) were largely different. The dispersion was much faster (t_c = 1.7 min) with the concrete containing the large particles than with the mortar (t_c = 31.0 min).

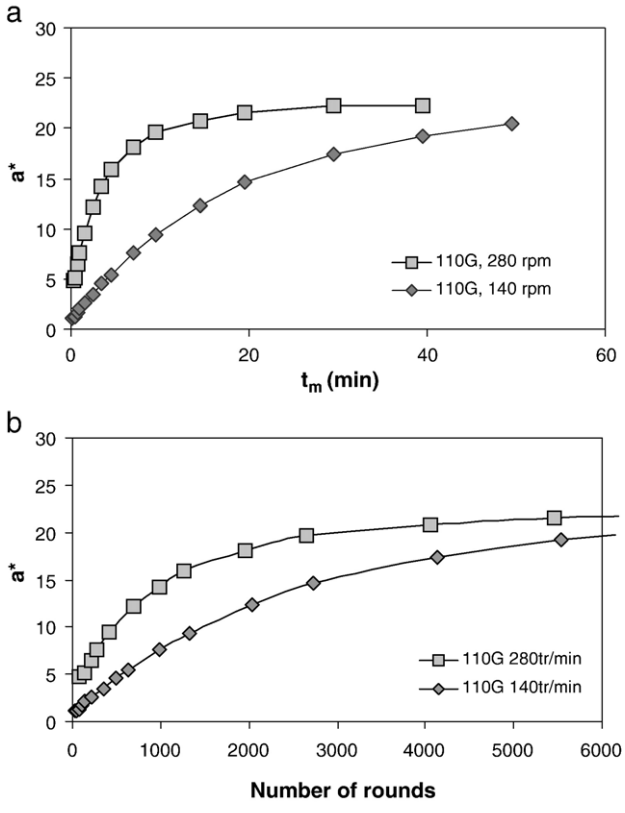

Fig. 6. Effect of the mixer rotation speed on a* for the 110G powder (MM1 mixer, 1l, "plastic" mortar). Mix design: mixture #2, described in Appendix A. (a) a* vs. time for two mixer speeds (280 and 140 rpm). (b) a* vs. deformation for two mixer speeds (280 and 140 rpm).

Table 1
Effect of the cohesion of the powder on the characteristic dispersion times: influence of the type of pigment on the r ratio for a mixer speed ratio of 2

Pigment powder	Ω_2/Ω_1	$r=t_{c1}/t_{c2}$
110 P	2	1.9
110 C	2	3.6
110 G	2	5

When two different mixers were used, selected among the *preferred* mixers for each application (MM1, 1L for mortar and CM1, 60L for concrete), the difference greatly dropped (t_c = 4.1 min for mortar and t_c = 1.7 min for concrete), but the trend remained favorable to concrete (Fig. 8). We can also point out the fact that a^*_{max} is similar in both (material, mixer) sets. This indicates completion of the dispersion process and that the same number of dispersed pigments were finally dispersed. Beyond this simple comparison, we can point out that, for standard mix designs of standard concrete and mortar, the mixing dispersion capability was always beneficial to concretes vs. mortars. There were no exception regardless of the mixers used. There is no doubt that the presence of larger aggregates in concrete remains essential to a greater dispersion capability. Therefore, the role of the particle size and of the concentrations of particles had to be studied further.

3.2. Effect of the volume fraction and the particle size

The volume fraction Φ_v occupied by the solids in concrete is of key importance in mechanical performances, and it is required to adjust the mix design so that a high volume fraction can be reached without greatly affecting the flow properties of the fluid material.

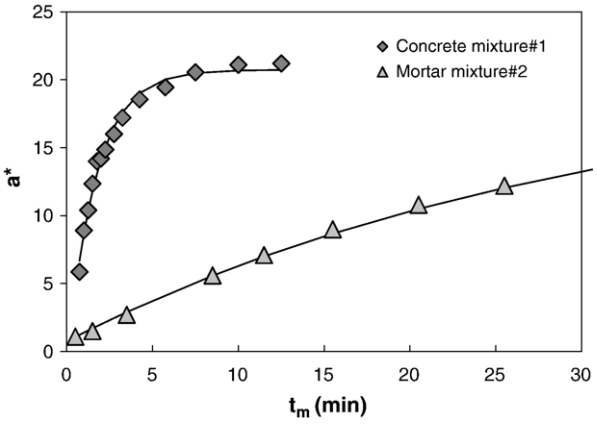

Fig. 7. Comparative example of the effect of the mixing time on a* for a reference mortar and a concrete in the same concrete mixer (CM2, 10l, 55 rpm, "plastic" mix designs as described in Appendix A).

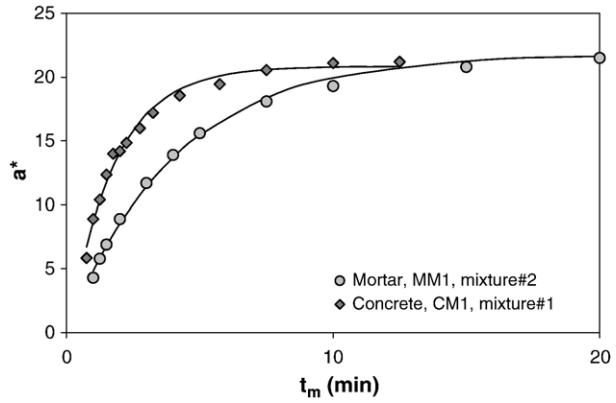

Fig. 8. Effect of the mixing time on a* for (a) "plastic" mortar in a mortar mixer (MM1, 1l, 280 rpm) and (b) "plastic" concrete in a concrete mixer (CM1, 40l, 55 rpm).

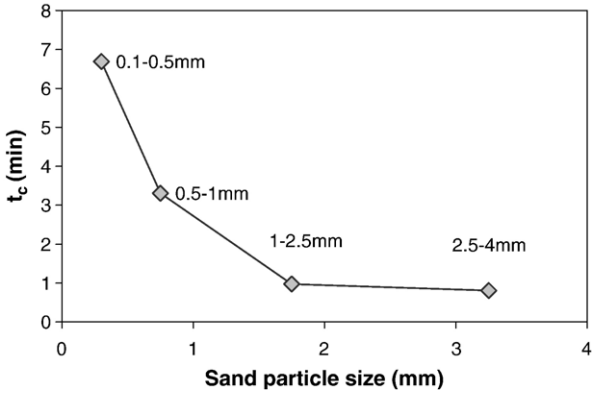

Fig. 10. Effect of the particle size for a constant volume fraction on the characteristic dispersion time (MM1 1l, 280 rpm). Mix designs: from mixture#3a through mixture#3d.

A series of mortars was prepared with the same solid ingredients to describe the effects of these two parameters. Φ_v was increased by changes of the sand content only. In these particular studies, the material contained one single class of sand. The mass water/cement ratio was maintained constant at 0.6, whereas the mixes were made up of peculiar mortars with identical cement slurries but different volume fractions of sand ranging from 10 to 60%. The evolution of t_c versus Φ_v for 3 sand sizes (Fig. 9) was clearly exponential, regardless the particle size.

Smaller particles were less efficient for dispersion, but the slopes became identical when size decreased. This was also confirmed by the results in Fig. 10, directly relating the dispersion time to the particle size for the same volume fraction (70% of solids). At the same Φ_v, reductions in particle diameters lead to an increased number of particles per volume unit N_p and to a smaller average inter-particle distance. Since the crushing mode for 110G cannot require predominantly viscous behaviors, frictional and collision mechanisms can be invoked to lighten these results. The preliminary results of Figs. 9 and 10 could suggest that the dominant dispersion mechanism of the pigment results from the collisions, driven by inertial effects, for the largest particles of the material, and might becomes partly frictional for the smallest. With this respect, the initial assumption that cohesive pigment is sensitive to the local solicitations imposed to the inter-aggregate paste by the largest particles remains valid.

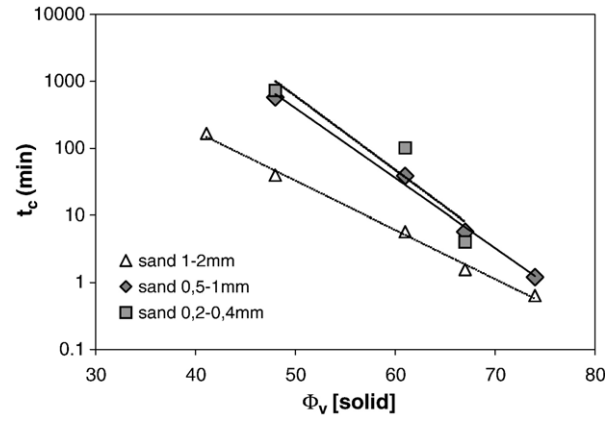

Fig. 9. Effect of the solid volume fraction on the characteristic dispersion time (MM1, 1l, 280 rpm), for different sizes of sand particles. Mix designs: (a) sand 1–2 mm: from mixture#4a through mixture#4e, (b) sand 0.5–1 mm: from mixture#5b through mixture#5e, (c) sand 0.2–0.4 mm: from mixture#6b through mixture#6d.

3.3. Effect of the mixer's rotation speed

The mixer's rotation speed of the mixers Ω was expected to play a major role on both distributive and dispersive mechanisms. It would seem logical that when speed increases, the a* plateau was reached faster. When the dispersion times t_c were compared, the effects of Ω on mortar (Figs. 11 and 12) and concrete (Fig. 12) were indeed very intense.

Comparison between Figs. 11 and 12 highlights the differences between mortar and concrete, earlier identified in Fig. 7. In mortars, the dispersion time was very high at a relatively low Ω; in such conditions, the stress imposed on the pigment aggregates during mixing was not very far from the stress required to break the particle cohesion. The probability of obtaining the appropriate conditions for particle rupture therefore dropped. Moreover, the frictional mode of energy dissipation was likely to be predominant at a low Ω. That was even more the case on the smallest particles in the mortars. For a higher Ω, the behavior was more similar for both materials (Fig. 12) reemphasizing the point that collision mechanisms are dominant at higher speeds.

Interpretation of the $t_c(\Omega)$ curves is not straightforward. Comparisons of the relative positioning of the curves is difficult without further information, particularly on energy dissipation during mixing. In both cases, the $t_c(\Omega)$ relationship fitted better with the power law curves with negative powers ranging between −2.3 and −1.6. The higher values in concrete indicated the higher sensitivity to the mixer speed.

In fact, another representation is better adapted and provides different insights to the speed effect. The kinetic evolution of a* (Eq. (1)) can be rewritten another way. Either versus time t:

$$a_t^* = a_{max}^* + (a_{min}^* - a_{max}^*) \times \exp(-k_c t), \quad (9)$$

where k_c is a characteristic dispersion rate (in min^{-1}),or versus deformation n_t:

$$a_t^* = a_{max}^* + (a_{min}^* - a_{max}^*) \times \exp(-Kn_t), \quad (10)$$

where $n_t = \Omega t$, $K = k_c/\Omega$ is a characteristic deformation rate,

When K is plotted versus the mixer's speed (Fig. 13), a linear correlation is experimentally observed, so that:

$$K = \alpha(\Omega - \beta), \quad (11)$$

this makes k_c dependent on the mixer's speed:

$$k_c = \alpha\Omega^2 - \beta\Omega \quad (12)$$

and eventually t_c:

$$t_c = \frac{1}{\Omega(\alpha\Omega - \beta)} \quad (13)$$

Parameter β is the x-axis intercept of the line in Fig. 13, and can be intuitively considered a "critical dispersion rate" related to cohesion of the cluster. It is possible to validate this intuition, because expression of the cluster cohesion index defined by Eq. (8) can be recalculated, by replacing the characteristic times t_{ci} by their expressions of Eq. (13). Thus:

$$i_c[\text{pigment}] = \frac{v_{ij}\Omega_i - \beta}{\Omega_i - \beta}, \text{ or } \beta = \frac{\Omega_i \times (i_c - v_{ij})}{(i_c - 1)} \quad (14)$$

β is therefore a growing function of the cohesion index and an increase of the cohesion index would also lead to higher critical stress needed to initiate particle breaking. On the other hand, α is independent of the cohesion of the pigment clusters.

It is worth pointing out that, at larger mixer speeds, the characteristic dispersion rate k_c is proportional to the square of the speed. It is easy to verify that the volume power consumption P/V when mixing viscous materials is also proportional to the square of the mixer speed if the "effective shear rate" inside the overall mixer volume is directly proportional to the rotation speed (Otto–Metzner hypothesis [17]), is experimentally valid for a very wide range of material/mixer pairs). Therefore, at a high mixer speed, the rate of dispersion would be proportional to the volume power consumption. This relationship was often seen on other products, such as carbon black agglomerates dispersed in elastomeric polymers [18].

Finally, series of experiments made at different volume fractions were obtained at three mixer speeds and for a single granular composition of 1–2 mm sands (Fig. 14). The relative position of the dispersion time vs. volume fraction lines shows some sensitivity to the mixer speed. The "slopes" in an exponential reference ranges between −0.12 and −0.17, and these lines appears as roughly parallel.

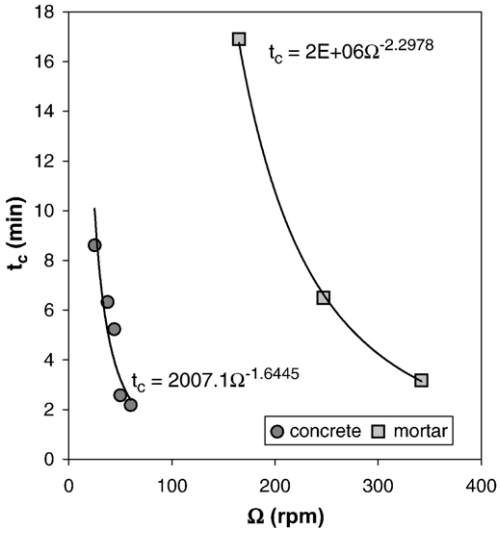

Fig. 12. Compared effects of the mixer's speed on characteristic dispersion times for concrete (CM1, 60l, 50 rpm) and mortar (MM1, 1l, 140 rpm). Mix design: mixture#2.

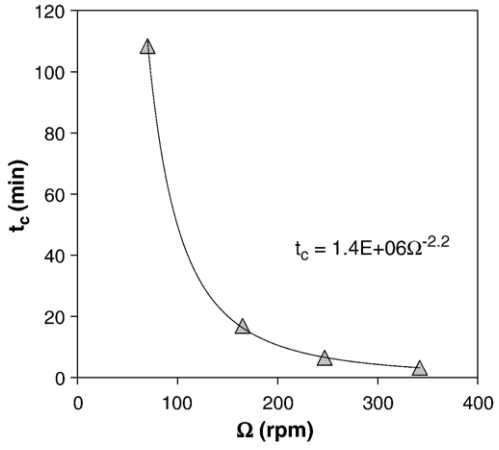

Fig. 11. Effect of the mixer's speed on characteristic dispersion times (MM2, 4l, plastic mortar). Mix design: mixture#2.

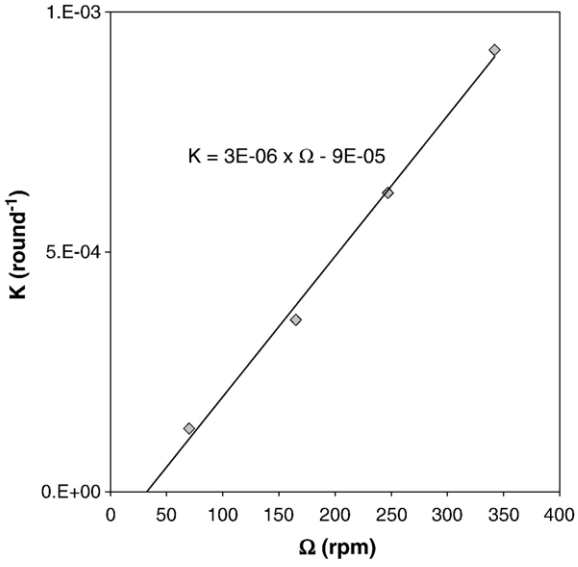

Fig. 13. Relationship between the characteristic deformation rate K and the mixer's speed (MM2, 4l, plastic mortar). Mix design: mixture#2.

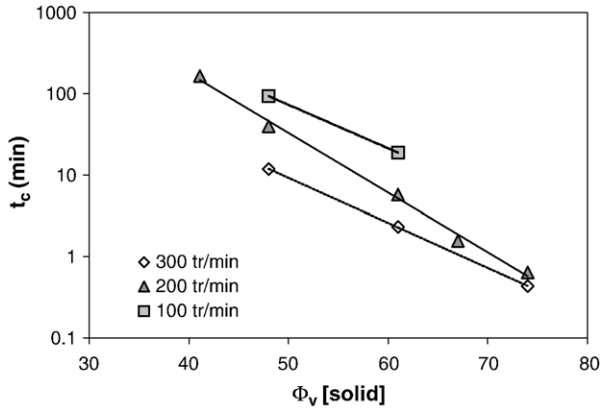

Fig. 14. Effects of the sand's volume fraction (one single class of particles 1–2 mm) for different mixer speeds (MM1, 1l). Mix design: from mixture#3a through mixture#3e.

3.4. Effect of the mixer's design

The cohesive pigment dispersion method can be applied to the selection of mixers. Obviously, the complete system, i.e. mixer geometry, including the design of the rotating equipment and the rotation mode (axial mixing or planetary mixing), the speed, the filled volume and the mix design must be considered simultaneously if the goal is to achieve a comparison of the mixers capabilities.

Certain key results pertaining to mortar and concrete mixers can be emphasized. Figs. 15 and 16 present these for some specific situations (mixer, mixer speed, volume), and for similar mortar or concrete mix designs.

For mortars (Fig. 15), we can mention that the most efficient mixer (MM3) is a laboratory device for which two mobiles were used simultaneously: the vessel rotates clockwise, while a turbine rotates simultaneously counterclockwise at relatively high speed (950 rpm). Its design is not adapted to concrete containing large particles. MM2 is a planetary mixer. Its geometry is roughly similar to the geometry of the MM1 laboratory mixers, but the accessible volume is about four times higher (4 l). Mixing efficiency is similar between the two. CM1, CM2 and CM3 mixers are specifically designed for concrete laboratory studies. In the CM2 and CM3 mixers, the vessel also rotates, and there is an additional low speed mobile, located half way between the wall and the center, rotating in the same direction. CM1 is equipped with counter-current, planetary, mixing devices with two mobiles, which is considered as efficient regarding the distribution of particles. CM4 is a relatively large scale mixer, with a complex geometry associated to the planetary motion of the auxiliary mixer. This study confirms certain aspects; for instance that dispersion is poor in concrete mixers when the larger aggregates are not present, which is known in civil engineering industries. The volume and mostly mixer speed have first order, non-linear, effects on the disaggregation capability.

For the concrete standard mix design used in the study (Fig. 16), the CM4 and the CM2 mixers are the most efficient, but no further conclusions can be drawn on the full intrinsic capability of the mixers, since distributive aspects are not consider here. With this respect, the rather poor result of the rotating drum mixer CM5 was expected because of the different mode of action of mixing, largely based on the action of gravity which imposes weak local solicitations on the slurry, but could favor distributive aspects.

In fact, the average shear rates used, and may be more importantly, the spatial uniformity of the shear produced in the experiments should be known for a proper interpretation of the results which remain currently comparative. If the former could be roughly evaluated through a ≪ Otto–Metzner ≫ type of macro approach, it is not directly possible to access the latter, which needs an approach at a micro scale. Even the determination of the relevant dimensionless numbers that could be used for comparison of the mixers, such as the Reynolds number, the Power of the Froude numbers, cannot be precisely achieved. Actually, the question should be inverted, and we could use the pigment

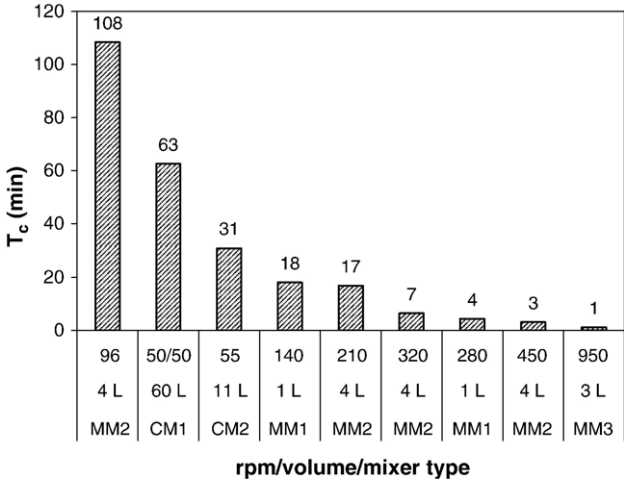

Fig. 15. Influence of the mixer for mortars: comparison of the characteristics dispersion time in several conditions (the first row in the *x*-axis legend corresponds to the mixer's speed, the second to the volume of mixed mortar and the third to the type of mixer).

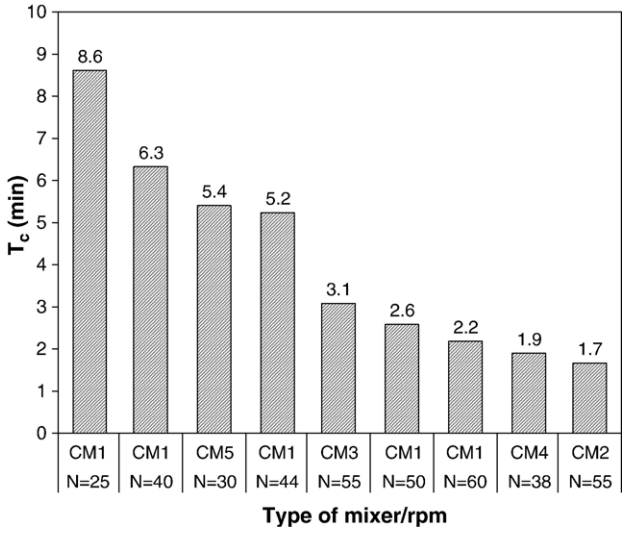

Fig. 16. Influence of the mixer for concrete; comparison of the characteristics dispersion time in several conditions (the first row in the *x*-axis legend corresponds to the mixer's type, the second to the mixer speed).

dispersion technique as a mean to access the local solicitations, including the local shear rates, imposed to the slurry.

4. Conclusion

A methodology was presented to set up mixing efficiency criteria for granular materials in terms of their dispersion capability. Instead of directly analyzing the evolution of the raw materials that are difficult to characterize during mixing, cohesive colored "spy" particles were added to the product prior to mixing. These particles are progressively disagglomerated under the effect of the solicitations imposed to the material during stirring, and measurements of the evolution of the intensity of the material red color over time provided a characteristic dispersion time that could be compared with each set of mix designs and mixing devices. The selected cohesive particles were granulated iron oxide pigments whose disintegration process during mixing was carefully examined. Currently, this approach provides certain mixing conditions, such as the mixer's speed, that make the dispersion times identical using different devices and possibly at different scales. Changes in mix designs could also be considered in the same manner.

At this point, this methodology opens opportunities to improve understanding of the mixing of highly concentrated granular materials such as concrete. Associated with in-situ rheological analysis available on laboratory equipment, and even with power consumption analysis carried out on industrial mixers, it should be possible to go beyond the macroscopic analysis of the flow that is usually made. This consider that the average shear rate inside a mixer is a key parameter in the determination of the mixer capability. The fact that small particles, with size similar to these products, are active tracers of what is going on at the particulate or interparticulate scale should contribute to the determination of *local* shear rates distributions. The word *local* refers here to the materials whose characteristic size has the same dimension as the tracer particle. In concretes and mortars, this concerns the intergranular cement paste. More generally the solicitations which contribute to the mixing efficiency could be probed with equivalent techniques. Assuming that the collision regime during concrete mixing is important and should be taken into account, at least after the water uniformly spreads through the mixer vessel, the kinetic energy of the large particles and the frequency of collisions between the largest aggregates could to be among the two other

Table 2
Composition of the mortar or cement mixtures used in the present study

Mixture # (all units in kg/m^3)	1 (concrete)	2 (micro concrete)	3a	3b	3c	3d	3e	3f	3g	3h	3i	3j	3k
Coarse aggregates (Cassis, France) 10/20	642												
Coarse aggregates (Cassis, France) 6/10	428												
Coarse aggregates (Cassis, France) 3/6	56												
Fine aggregates (Cassis, France) 2.5/4	243	443		(0%)		1182 (100%)	148 (13%)	222 (19%)	296 (25%)	367 (31%)	443 (38%)	591 (50%)	887 (75%)
Fine aggregates (Cassis, France) 1/2.5	81	148			1182								
Fine aggregates (Cassis, France) 0.5/1	81	148		1182			1035	961	887	815	739	591	296
Fine aggregates (Cassis, France) 0/0.5	243	443	1182										
Cement CEMI 52.5 CP2 (Le Teil, France)	280	500	500	500	500	500	500	500	500	500	500	500	500
Limestone Filler (St Beat, France)	162	296	296	296	296	296	296	296	296	296	296	296	296
Admixture lignosulfonate (Chryso)	1	0.5											
Water (Water/Cement=0.6)	170	300	300	300	300	300	300	300	300	300	300	300	300
Red pigment (Bayer)	2	4	4	4	4	4	4	4	4	4	4	4	4

Mixture # (all units in kg/m^3)	4a	4b	4c	4d	4e	5b	5c	5d	5e	6b	6c	6d
Fine aggregates (Palvadeau, France) 1/2	256 (10%)	512 (20%)	654 (40%)	1280 (50%)	1536 (60%)							
Fine aggregates (Palvadeau, France) 0.5/1						512 (20%)	654 (40%)	1280 (50%)	1536 (60%)			
Fine aggregates (Palvadeau, France) 0.2/0.4										512 (20%)	654 (40%)	1280 (50%)
Cement CEM I 52.5 CP2 (Le Teil, France)	980	872	763	545	436	872	763	545	436	872	763	545
Water (E/C=0.6)	590	590	300	300	300	590	300	300	300	590	300	300
Red pigment (Bayer)	8	6	5	4	3	6	5	4	3	6	5	4

most significant parameters contributing to energy dissipation. The preliminary results shown in this paper also prove the interest of simplifying the problem by the use of either mono-modal systems, possibly made of glass beads or simpler sand or filler particles. This should help finding some of the mixing fundamentals of granular materials. Finally, it is necessary to keep in mind that, at all scales, the distributive aspects remain extremely important for mixing efficiency. The tracer techniques, even with cohesive particles, can also be used for simplified determination of the distributive capability, even though further practical challenges have to be addressed, more specifically those related to sampling and statistics.

Notation

β	x-intercept of the characteristic deformation rate vs. mixer speed line
η	viscosity, Pa s
$\dot{\gamma}$	shear rate, s^{-1}
Ω	mixer speed, rpm
Φ_v	solid volume fraction
σ	shear stress
χ_d	mixing efficiency coefficient
a^*	red color intensity measured as a component of the L*a*b* standards
a^*	a^* at time t
a^*_{min}	virtual minimum value of a^* at $t=0$
a^*_{max}	maximum value of the a^* vs. time curve
i_c	cohesion index
K	characteristic deformation rate, min^{-1}
k	proportionality constant
k_c	characteristic dispersion rate, min^{-1}
k_2	proportionality constant
Nb_t^c	number of debris per volume unit resulting from crushing at time t
Nb_t^r	number of clusters per volume unit remaining at time t
N_p	number of particle per volume unit
n_t	deformation
P	power consumption
R_0	cluster size at time $t=0$
R_1	ratio of the total added water for pre-wetting
R_2	ratio of the total added water after wetting
R_t	cluster size at time t
r	characteristic dispersion time ratio
S2	percentage of surface area occupied by the uncrushed particles
t	time
t_c	characteristic dispersion time of pigment clusters, min
t_{c0}	characteristic dispersion time of pigment clusters in absence of particules, min
t_m	mixing time after total water additions
v	mixing speed ratio
V	volume

Acknowledgements

The authors are grateful to acknowledge the technicians who participated in the practical realization of the experiments for

Table 3
Concrete and mortar mixers used in the present study

Concrete mixers	
CM1 Counter-current mixers, "planetary" motion (pan fixed/scraper moving/shaft rotating) Usual rotation speed: 25–80rpm Mixing capacity: 80 L	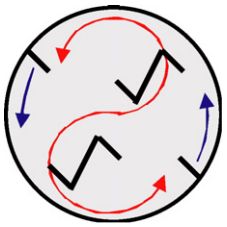
CM2 Co-current motion (same rotation direction) (pan rotating/scraper fixed) Usual rotation speed: 55 rpm Mixing capacity: 30 L	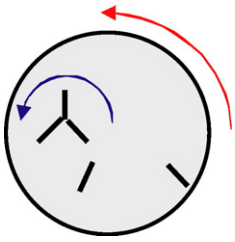
CM3 Co-current motion (same rotation direction) (pan rotating/scraper fixed) Usual rotation speed: 55 rpm Mixing capacity: 50 L	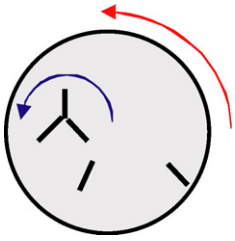
CM4 Main axial mixer, with scrapers for bottom, axis and wall. Freely rotating auxiliary mixer Usual rotation speed: 25–40 rpm Mixing capacity: 200 L	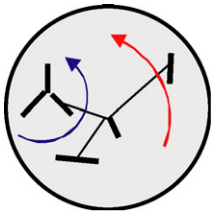
CM5 Drum mixer Usual rotation speed: 30 rpm Mixing capacity: 170 L	(blank)
Mortar mixers	
MM1 Planetary motion Usual rotation speed: 140–280 rpm Mixing capacity: 1 L	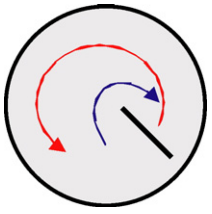
MM2 Planetary motion Usual rotation speed: 70–380 rpm Mixing capacity: 4 L	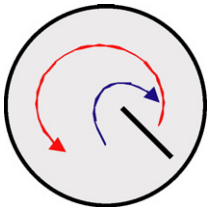

Table 3 (*continued*)

Concrete mixers	
MM3 Intensive mixer Type R Center shaft (pan rotating/scraper fixed) Usual rotation speed: 950–3800 rpm Mixing capacity: 3 L The shaft and the pan are tilted	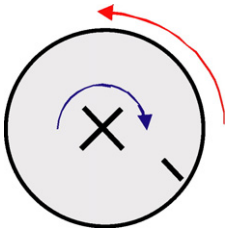

which results are described in this document: Marie Bayle, Olivier Refouvelet and Caroline DaSilva.

Appendix A. Mix designs for mortar and concrete

The mix designs of cementitious materials require using of a wide range of particles. Our study is only devoted to conventional concretes. Particles were never larger than 20 mm (aggregates). The smallest were cement particles (typically 50 μm), that is a relatively polydispersed material. Fillers were occasionally used to fill or complete the wide granular distribution. Water was occasionally admixtured with plasticizers (lignosulfonate).

The first column of Table 2 indicates, unless otherwise noted, the nature of the particles, the sizes of the smallest particle and the sizes of the largest particles, as well as the origin of the particles. The other columns indicate the composition of the mixtures in kg/m^3 as indicated in the figures given in the main text.

Appendix B. Mixer designs

This appendix describes the main features pertaining to the mixers used in this study (Table 3). All are laboratory or pilot scale devices, customarily used for concrete (referenced as CM) or mortars (referenced as MM).

References

[1] Y. Charonnat, H. Beitzel, RILEM TC 150 ECM, Efficiency of concrete mixers; report: efficiency of concrete mixers towards qualification of mixers, Mater. Struct. 30 Suppl. 196 1997, 28–32.
[2] A. Johansson, The relationship between mixing time and the type of concrete mixer, Natl. Swed. Build. Res. Summaries T1 (1971) 1971.
[3] P.O. Vandanjon, F. de Larrard, B. Dehousse, G. Villain, R. Maillot, P. Laplante, Homogénéisation des bétons en centrale de fabrication discontinue, Bull. Lab. Ponts Chaussees 228 (2000) 35–46.
[4] D. Chopin, F. de Larrard, B. Cazacliu, Why do HPC and SCC require a longer mixing time, Cem. Concr. Res. 24 (2004) 2237–2243.
[5] P. Robin, Contribution to the characterization of the granular mixes sample with aview to examine the mixing phenomena, Thèse de l'Université Blaise Pascal, Clermont-Ferrand, 1988.
[6] D.A. Williams, A.W. Saak, H.M. Jennings, The influence of mixing on the rheology of fresh cement paste, Cem. Concr. Res. 29 (1991) 1491–1496.
[7] H.-S. Lee, J.-Y. Lee, M.-Y. Yu, Influence of inorganic pigments on the fluidity of cement mortars, Cem. Concr. Res. 35 (2005) 703–710.
[8] T.C. Powers, The Properties of Fresh Concrete, John Wiley & Sons, New York, 1968.
[9] V. Collin, Rheo-optical study of carbon black dispersion in elastomers, Thèse de doctorat en Science et génie des matériaux , Ecole des Mines de Paris, Sophia-Antipolis, 2004.
[10] G. Teichmann, Colorimétrie dans l'industrie du béton, Betonw. Fert.tl.-Tech. 11 (1990) 58–73.
[11] L. Struble, R. Szecsy, W.G. Lei, G.K. Sun, Rheology of cement paste and concrete, Cem.Concr. Aggr. 20 (2) (1998) 269–277.
[12] S.P. Rwei, D.L. Feke, I. Manas-Zloczower, Observation of carbon black agglomerate dispersion in simple shear flows, Polym. Eng. Sci. 30 (1990) 701–706.
[13] V. Collin, E. Peuvrel-Disdier, Dispersion mechanisms of carbon black in an elastomer matrix, Elastomery 9 (2005) 9–15 (N°special, June).
[14] S.V. Kao, S.G. Mason, Dispersion of particles by shear, Nature 253 (1975) 619–621.
[15] R.L. Powell, S.G. Mason, Dispersion by laminar flows, AIChE J. 28 (1982) 286–293.
[16] S.P. Rwei, D.L. Feke, I. Manas-Zloczower, Characterization of carbon black dispersion by erosion in simple shear flows, Polym. Eng. Sci. 31 (1991) 558–562.
[17] A. Metzner, R. Otto, Agitation of non newtonian fluids, AIChE J. 3 (1957) 3–10.
[18] I. Manas-Zloczower, Model and analysis of kinetics erosion in simple shear flows, Rubber Division Meeting, Savannah, Georgia, April 28–May 1 2002, 2002.